Dynamics of Membrane Nanotubulation and DNA Self-Assembly

T. Roopa,* N. Kumar,* S. Bhattacharya,† and G. V. Shivashankar*‡
*Raman Research Institute, Bangalore, India; †Tata Institute of Fundamental Research, TIFR, Mumbai, India; and ‡National Center for Biological Sciences, TIFR, Bangalore, India

ABSTRACT A localized point-like force applied perpendicular to a vesicular membrane layer, using an optical tweezer, leads to membrane nanotubulation beyond a threshold force. Below the threshold, the force-extension curve shows an elastic response with a fine structure (serrations). Above the threshold the tubulation process exhibits a new reversible flow phase for the multilamellar membrane, which responds viscoelastically. Furthermore, with an oscillatory force applied during tubulation, broad but well-resolved resonances occur in the flow phase, presumably matching the time scales associated with the vesicle-nanotubule coupled system. These nanotubules, anchored to the optical tweezer also provide, for the first time, a direct probe of the real-time dynamics of DNA self-assembly on membranes. Our studies are a step in the direction of analyzing the dynamics of membrane self-assembly and artificial nanofluidic membrane networks.

INTRODUCTION

Membrane tubules are ubiquitous in soft-matter and biological systems (Sheetz, 2001) and result from applying a localized force perpendicular to the surface of the membrane (Evans and Yeung, 1994; Roopa and Shivashankar, 2003). Such tubulation processes have important implications within biological cells (Hochmuth et al., 1996; Hirschberg et al., 1998; Waters and Pfeffer, 1999; Roux et al., 2003), and also provide a framework for realizing artificial nanofluidic membrane networks (Evans et al., 1996; Chiu et al., 1999; Karlsson et al., 2001; Karlsson et al., 2002). Micromanipulation experiments on both artificial and biological membranes have opened up new possibilities for understanding the underlying physical properties in detail (Waugh and Hochmuth, 1987; Evans and Rawicz, 1990; Barziv and Moses, 1994; Derenyi et al., 2002; Powers et al., 2002). Specifically we had measured, using an optical tweezer, the force of tubule formation, which exhibited an interesting viscoelastic membrane-flow regime, beyond the initial elastic regime (Roopa and Shivashankar, 2003). However all of the above experiments have only addressed the mechanics of tether formation in the context of both artificial and natural membranes.

In this article, we explore, for the first time, the dynamics of membrane tubulation from multilamellar vesicles, using an optical-trap modulation technique in conjunction with the force-extension measurements reported earlier. A detailed analysis of the force-extension (F-X) curves, below the tubulation threshold, reveals a robust phenomenon of ''serrations''. The frequency response shows broad but well-resolved resonances at characteristic frequencies for a fixed tubule extension, beyond the tubulation threshold. Moreover, the variation of the response amplitude as a function of extension shows characteristic frequency dependent peaks near the tubulation threshold. We also show, for the first time, that membrane nanotubules tethered with a trapped bead provide an excellent probe of the real-time dynamics of DNA self-assembly (Saffinya, 2001).

EXPERIMENTAL METHODS

Fig. 1 is the schematic of our experimental arrangement. An infrared laser (830 nm, GaAlAs diode, model 5430; SDL., San Jose, CA) is focused to a diffraction limited spot of diameter $\sim$0.5 μm, using a high numerical aperture oil immersion objective (Olympus 100×, 1.4 N.A., Japan) mounted on an inverted microscope (Olympus IX70). For the frequency sweep measurements, a 0.5 V sinusoidal signal from the DAQ board (model: PCIMIO16XE-10; National Instruments, Austin, TX) generated at different frequencies by Lab View (National Instruments) programming is connected to the laser diode power supply for modulating the trap. The signal from the DAQ board also serves as the reference for the phase-sensitive measurements. The response amplitude dependence on the tubule extension is measured, by a lock-in amplifier (SR830 Stanford Research Systems, Sunnyvale, CA), whose reference output is connected to the laser diode. Single particle backscattering of a red laser by the trapped 2 μm diameter polystyrene bead is focused onto a quadrant photodiode (SPOT4D; UDT Instruments, Baltimore, MD) to detect the displacement and hence the force (Roopa and Shivashankar, 2003). The output of the quadrant photodiode amplifier (X-Y Position Indicator Model 431; UDT Instruments) is fed to the lock-in amplifier to measure the response amplitude at the modulation frequency (1 Hz to 200 Hz). An appropriate integration time is chosen at each step of extension, in order to integrate out the Brownian fluctuations of the bead. In our experiments, the trap stiffness is $\sim 1 \times 10^{-5}$ N/m (for 40 mA laser diode current) and varies in the range of 0.6×10^{-5} N/m to 1.8×10^{-5} N/m with the modulating signal of 0.5 V. The data is acquired using the DAQ board and Lab View 5.1. The sample is mounted on a PZT stage with nanometer precision (three-axis PZT stage model: P577.3CL, with servo controller model: E-509.C3; Physik Instrumente, Palmbach, Germany). For constant force measurements, the output of the quadrant amplifier is used as the feedback signal for PZT translation stage (Fig. 1).

The output of the quadrant detector amplifier is a voltage signal (1 volt output from the quadrant detector amplifier corresponds to $\sim$0.6 μm displacement of the bead). The amplifier gives two outputs corresponding to the bead displacement in perpendicular directions in the focal plane (V_x and V_y). We chose the direction in which the tubule is pulled out. This voltage is

Submitted December 24, 2003, and accepted for publication March 30, 2004.
Address reprint requests to G. V. Shivashankar, E-mail: shiva@ncbs.res.in.

0006-3495/04/08/974/06 $2.00
doi: 10.1529/biophysj.103.039297

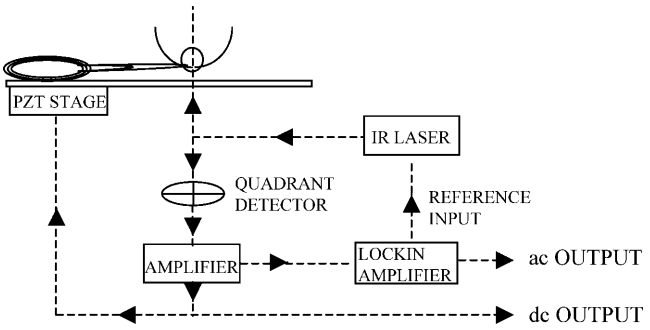

FIGURE 1 Schematic of the experiment. The optically trapped bead is used to tubulate the vesicle adhered on the coverslip mounted on the PZT stage. The force of tubulation is monitored using a photosensitive quadrant detector and amplifier. The amplifier output is fed to the lock-in amplifier to obtain the response amplitude. The amplifier output is the feedback to the PZT stage for constant force measurement of DNA assembly.

fed into the lock-in amplifier that convolutes the signal with the reference signal to give the phase-sensitive response of the bead at the frequency of modulation. The lock-in amplifier gives the imaginary (V_I) and real (V_R) components of the response at the modulating signal frequency, from which the amplitude ($V_A = (V_R^2 + V_I^2)^{1/2}$) and the phase ($\hat{A} = \tan^{-1}(V_I/V_R)$) of the bead oscillation are calculated.

The DDAB (didodecyl dimethyl ammonium bromide) vesicles are prepared by the hydration method, described earlier (Roopa and Shivashankar, 2003). The final concentration of the lipid molecules is ~4 mM in PBS (phosphate buffer saline, 2× buffer, pH 7.4). This method of preparation gives multilamellar vesicles with sizes ranging from 5 μm to 25 μm in diameter. We select an isolated vesicle stuck firmly on the coverslip for our experiments. The optically trapped carboxylated bead is attached to the cationic vesicle adhered onto a glass coverslip, by electrostatic interactions. Force-extension curves are recorded by measuring the displacement from the trap center of the trapped bead as a function of tubule extension using the PZT stage. An analog output signal from the data acquisition board is used to control the PZT stage.

RESULTS AND DISCUSSION

Force-extension curves of tubulation

In Fig. 2, we plot the force-extension curve of the membrane tubulation, to demonstrate its reversibility. The experimentally measured force-extension curves reveal a sharp increase in the force required to pull out a tubule from the multilamellar membrane vesicle (Roopa and Shivashankar, 2003). Beyond a threshold force ~0.6 pN, however, the tubule length can be increased to several tens of microns with <0.2 pN increase in the force. As clearly seen, the force-extension curves display no hysteresis in the force of tubule formation and retraction, the velocity of tubule formation being ~200 nm/s. Two regimes can be seen in the force-extension curve, the initial stiff elastic regime where the force increases sharply, and the late saturation regime, which is considerably softer. The characteristic spring constants (dF/dX) in the two regimes are vastly different: $\sim 1 \times 10^{-3}$ pN/nm in the stiff elastic regime and $\sim 2.5 \times 10^{-6}$ pN/nm in

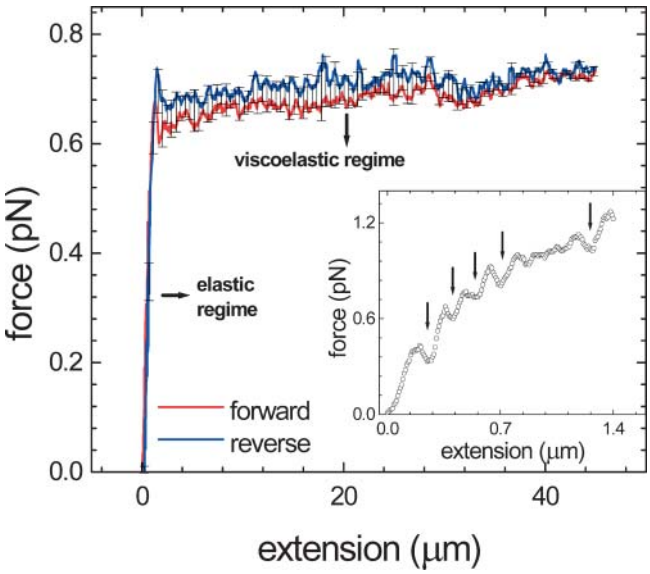

FIGURE 2 Force-extension curve (extension rate ~200 nm/s) for a typical membrane tubulation process. The two regimes are marked as elastic and viscoelastic. The forward and the reverse data lie within the error bars, suggesting a largely reversible response. Inset shows the elastic regime of a typical, but different vesicle, force-extension curve with the serrations (marked by *arrows*). The decrease in the force at such serrations is of the order of 0.1 pN.

the soft regime (in the linear approximation). Fig. 2 shows two new important results. First, the response is largely reversible as shown by the close correspondence between the forward and reverse F-X cycles. In addition, the elastic regime shows characteristic serrations in the F-X curve as shown in the inset to Fig. 2, with the raw data smoothened by an adjacent eight point averaging. An average number of two or three such serrated jumps (of the order of 0.1 pN as shown by arrows in Fig. 2, *inset*) were observed over different vesicles. It may be noted, however, that the inset refers to a different but similar vesicle for which the threshold force is ~1 pN. The force-extension curve is, broadly speaking, robust and reproducible, but the fine structures (serrations) are not reproducible in detail, although serrations appear in each case. All measurements have been done at some specific but randomly chosen anchoring site on the vesicle (for a given bead and vesicle). At this stage the microscopic origins of the serrations in the F-X curve are unclear. Plausible explanation for the observed serration may be a), stick-slip motion between the bilayers of the multilamellar vesicle during tubulation; or b), successive breakages of the vesicle-bead adhesive contacts.

Fig. 3 shows the force-extension curves of tubule formation for different pulling rates (500 nm/s, 200 nm/s. and 20 nm/s). The saturation regime is characteristic of flow (tubulation) of the multilamellar vesicle material under an applied tension beyond the threshold. As noted above, the flow here is reversible and independent of the rate of

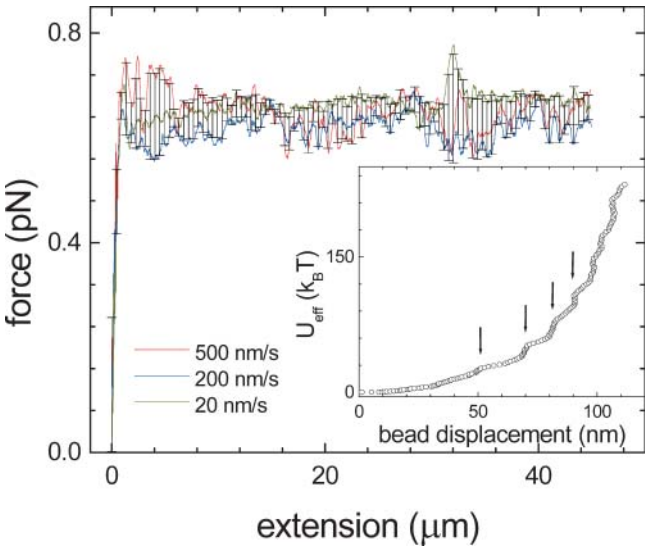

FIGURE 3 Force-extension curves are independent of the rate of tubulation (500 nm/s, 200 nm/s, and 20 nm/s). Inset shows the effective potential derived from the elastic regime of the experimentally measured force-extension curve; arrows mark the steps arising due to the serrations in the force-extension curve.

tubulation. The nature of the curve does not change when the tubule is formed many times and is very reproducible. Also, the effective potential, which is the sum of the trap potential and the tubule potential, does not vary with the rate of tubule formation. We extracted the effective potential seen by the bead during the tubule formation from the experimental F-X data (Fig. 2). The bead is displaced from the trap center due to the force of tubulation of the vesicle. Hence, the actual length of the tubule is the difference between the distance moved by the vesicle bearing PZT stage and the displacement of the bead in the trap. Since, however, the tubule length is of the order of micrometers, whereas the displacement of the bead is of the order of nanometers, we approximate the length of the tubule to the distance moved by the PZT stage. (The optically trapped bead is just a probe then to monitor the tubule extension). Thus, integrating the rising part of the curve gives us the potential plotted in inset to Fig. 3. The effective potential U_{eff} seen by the bead is a sum of the potential arising due to trap U_{tr} (harmonic) and the tubule extension U_{tb} (anharmonic). As can clearly be seen, we observe steps in the effective potential corresponding to the serrated fine structure in the force-extension curves. (In our experiment, the tubule radius, $r = f/\pi\sigma =$ 80 nm, where $f = 0.6$ pN is the threshold tubulation force and $\sigma = 2.6 \times 10^{-6}$ N/m is the measured membrane tension (Roopa and Shivashankar, 2003). The membrane bending rigidity modulus $B = fr/2\pi \sim 8 \times 10^{-21}$ Nm, where the tubule radius $r = 80$ nm and the tubulation force f is ~0.6 pN.) The operating point on the force-extension curve so obtained now determines the dynamics of the tubulating membrane as discussed below.

Probing the dynamics of the tubulating membrane: frequency response

The coupled system of the tubulating multilamellar membrane and the optically trapped bead was probed for its dynamics (for frequency response) by weakly modulating the optical trap stiffness at chosen frequencies that creates an alternatively shallow and deep potential well for the bead to move in. The bead is displaced from the trap center due to the tension of the tubule coupled to it. Thus the linear system response was measured by the (small) amplitude of bead oscillations as a function of frequency.

In Fig. 4 we plot the response (the amplitude of bead oscillations) as a function of the frequency of trap modulation for a constant tubule extension of 5 μm in the saturation regime of the force-extension curve. The frequency is varied from 1 Hz to 200 Hz in steps of 1 Hz; with a wait time of 5 s before the data is recorded after a step change in frequency. Also shown is the response amplitude of a trapped bead that is not anchored to the tubule. It is clearly characteristic of an overdamped oscillator. The small but discernible peak structure riding the response is to be expected from the nature of excitation, namely that we have here a parametric modulation of the trap stiffness (multiplicative force) rather than an (additive) externally applied periodic force as described by the Mathieu equation. The particle in the trap, therefore, exhibits the nonlinear beat phenomena. In Fig. 4, for the bead anchored to the tubule, we can see three broad but measurable peaks in the response amplitude versus frequency curve, at ~20 Hz, ~70 Hz, and ~140 Hz with the relative amplitudes (a.u.) being ~0.75, ~0.3, and ~0.15, respectively.

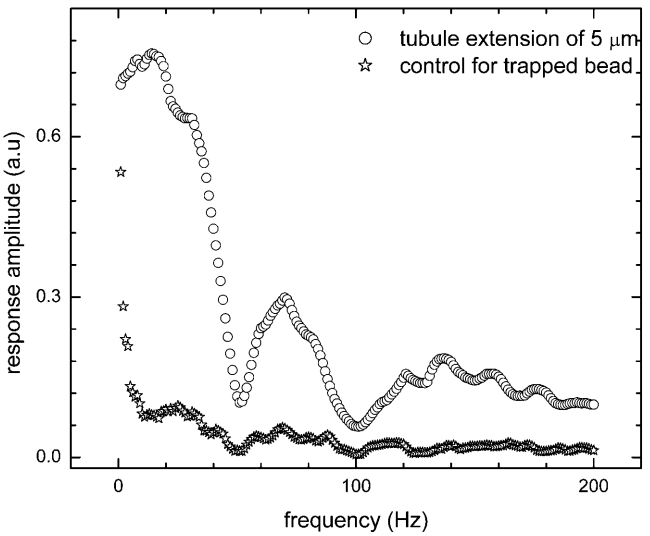

FIGURE 4 Response amplitude as a function of frequency of modulation at a tubule extension of 5 μm (close to the onset of saturation in the force-extension curve). The frequency is varied from 1 Hz to 200 Hz in steps of 1 Hz, with a wait time of 5 s before the data is recorded after a step change in frequency. The frequency response for a trapped bead not anchored to the tubule is also plotted as control.

A possible explanation for the observed resonance may be due to the Raleigh oscillations of the vesicle, driven by its surface tension. In that case, the resonant frequencies are given by (Landau and Lifshitz, 1959),

$$\omega^2 = Al(l-1)(l+2),$$

where $A = \alpha/\rho R^3$, with α the surface-tension coefficient, ρ the density, and R the radius of the vesicle. Here l takes the values of positive integers. $l = 0$ is not allowed since this would result in increase in the volume of the drop and the fluid is incompressible. So is $l = 1$ which results in translational motion of the drop. The dominant even order oscillation frequencies are; for $l = 2$, $\omega_2^2 = 8A$, for $l = 4$, $\omega_4^2 = 72A$, and for $l = 6$, $\omega_6^2 = 240A$, which gives the frequency ratios 1, 3, and 5.5, respectively. The resonant peaks observed in the Fig. 4 are approximately in the same ratio as noted above. However a precise characterization of the harmonics is difficult at this stage.

Response amplitude as a function of tubule extension

In Fig. 5, we plot the response amplitude as a function of tubule extension with a wait time of 2 s before each step change in extension (step size of 200 nm), at different trap modulation frequencies (20 Hz, 45 Hz, 80 Hz, and 100 Hz) on the same vesicle. The force-extension curve is also plotted to show that the saturation of the amplitude corresponds to the saturation in the force-extension curve. The amplitude of the response increases with the tubule length and saturates at an extension in the range 2–5 μm (varies for different vesicles). At frequencies of 80 Hz and 100 Hz we see a resonance at the onset of saturation at tubule extensions of 3.5 μm and 2.5 μm, respectively. In the saturation region of the force-extension curve, the displacement is almost constant resulting in the saturation of the response function. The saturation values for different frequencies of modulation follow the response obtained in the frequency sweep measurements (Fig. 4). Thus, for example, the response amplitude in the saturation regime decreases from 20 Hz to 50 Hz and again peaks at 80 Hz. Further, there is a resonant enhancement of the response amplitude at the transition from elastic to the viscoelastic region of the force-extension curve. The peak height is maximal at 80 Hz and decreases at 100 Hz (Fig. 5), revealing a characteristic frequency range where the time scale of membrane flow presumably matches the oscillation in the bead displacement.

Membrane nanotubule as a probe of the dynamics of DNA self-assembly

In Fig. 6 we plot the real-time dynamics of DNA self-assembly on tethered membrane nanotubules. We show here

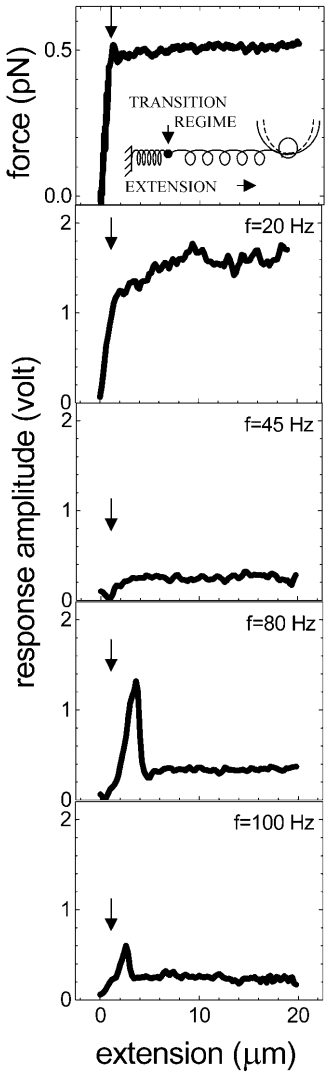

FIGURE 5 Response amplitude as a function of tubule extension for modulation frequencies (20 Hz, 45 Hz, 80 Hz, and 100 Hz). The force-extension curve is also plotted to depict the correlation between the onset of flow regime and the resonance in the amplitude response.

that the integration dynamics is independent of the contour length of the DNA molecules. DNA assembly on the tubule is probed by anchoring it to the trapped bead that is held at a constant force by a feedback loop. The tubule is extended to $\sim$15 μm from the vesicle adhered on the coverslip, where we are in the saturation regime of the force curve and the bead is held at a constant force $\sim$0.3 pN. The bead position is continuously monitored on the position sensing quadrant photodiode using the backscattered red laser. The length of the tubule changes as a consequence of the rupture of the membrane bilayer, due to the condensation of the DNA molecules. This results in an increase in force on the bead, hence a shift in its mean position in the trap. The difference in the two mean positions is the feedback to the PZT stage to compensate for the change in length. Since the trapped bead is a Brownian particle, its mean position in the trap fluctuates

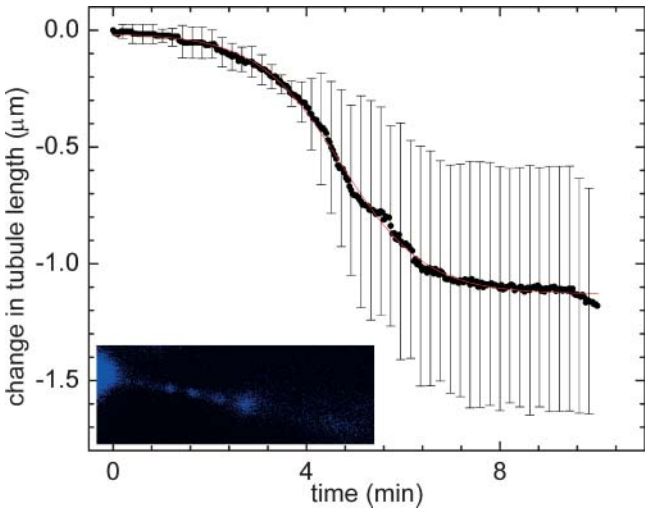

FIGURE 6 Plot of the dynamics of DNA self-assembly on the membrane nanotubule as a function of time (recorded using constant force trap measurement). Change in length of the tubule is found to be independent of the size of the DNA molecules (100 bp, 5 Kbp, and 48 Kbp). Inset shows a fluorescence picture of the DNA stained with YOYO dye assembled on the membrane tubule.

and hence the feedback is activated only when the shift in the mean position is greater than four times the standard deviation of the fluctuations.

Fig. 6 shows that the DNA assembly curves are similar (and fall within the range shown in the figure) for 100 bp, 5 Kbp, and 48 Kbp sizes. There is an initial slow rate of decrease in length for ~4 min, in this phase all the sizes show the same rate. During the time from 4 min to 7 min the rate is exponential over which the length decreases by ~1 μm before it saturates. The exponential rate of decrease continues for much longer lengths (up to 7 μm) in some cases.

The condensing DNA molecules recruit the lipid molecules of the tubule membrane bilayer to neutralize their charge and release the counterions. DNA, being a negatively charged polymer with a high charge density, assembles on cationic membrane bilayers. This process, driven by electrostatic interactions, is a self-assembling process. The increase in entropy, due to counterion release as a result of the DNA condensation on the membrane, more than offsets the decrease in entropy due to the DNA condensation itself. The cationic surfactant molecules of the vesicle neutralize the charge on the DNA and hence coat the DNA. With increase in the DNA concentration on the membrane more surfactant molecules are pulled out of the bilayer. The membrane bilayer is slowly ruptured resulting in the decrease in the tubule length (Fig. 6). Eventually the vesicle is completely ruptured and we observe DNA-lipid complexes under the microscope. Hence there is a slow breakdown of the bilayer leading to a decrease in the tubule length. The plots show that the dynamics of the assembly, at its onset and during the rapid decrease in length, is independent of the size of the DNA molecules. With time the variation between the curves, obtained for different DNA sizes on different vesicles, increases probably due to the variability in the vesicles.

The initial slow phase of decrease in tubule length is when the DNA molecules nucleate at different points along the tubule. When the nuclei start to grow, there is a rapid decrease in length of the tubule, after which the rate of decrease saturates and eventually the tubule breaks. The assembly curves fit to a sigmoidal curve, with a variation in the rates in the exponential regime. For the sigmoidal fit shown in the Fig. 6, the assembly rate ~0.3 μm/s. Inset to Fig. 6 shows fluorescence image of the DNA assembled on the tubule. The DNA molecules are stained with YOYO dye at a concentration of 1 molecule of YOYO per 5 base pairs of DNA. The DNA molecules nucleate at different points on the tether, and the intensity of each of these nuclei grows with more molecules concentrating at these points, before the tubule breaks.

CONCLUSION

In summary, we have presented the dynamic response of a novel flow regime during membrane tubulation. For the first time we see evidence of a resonance during tubulation which may provide insights into, both the surface tension of the vesicle as well as the dynamics of lipid hopping between membrane bilayers. The force-extension curves are shown to be broadly reversible and independent of tubulation rate. In addition, they reveal characteristic ''serrations'' in the stiff elastic regime of the F-X curve. We have also demonstrated a new application of these tethered membrane nanotubules, namely as biosensors to probe the real time dynamics of DNA self-assembly. Our work is in the direction of probing the dynamical peristaltic modes of a membrane tubule that may have implications for the propulsion of large biomolecules through the nanotubules and for microfluidics in general.

We thank Y.Hatwalne and Madan Rao for useful discussions.

REFERENCES

Bar-Ziv, R., and E. Moses. 1994. Instability and ''pearling'' states produced in tubular membranes by competition of curvature and tension. *Phys. Rev. Lett.* 73:1392–1395.

Chiu, D. T., C. F. Wilson, F. Ryttsen, A. Stromberg, C. Farre, A. Karlsson, S. Nordholm, A. Gaggar, B. P. Modi, A. Moscho, R. A. Garza-Lopez, O. Orwar, and R. N. Zare. 1999. Chemical transformations in individual ultrasmall biomimetic container. *Science*. 283**:**1892–1895.

Derenyi, I., F. Julicher, and J. Prost. 2002. Formation and interaction of membrane tubes. *Phys. Rev. Lett.* 88:238101-1–238101-4.

Evans, E., and W. Rawicz. 1990. Entropy-driven tension and bending elasticity in condensed-fluid membranes. *Phys. Rev. Lett.* 64:2094–2097.

Evans, E., and A. Yeung. 1994. Hidden dynamics in rapid changes of bilayer shape. *Chem. Phys. Lipids*. 7:39–56.

Evans, E., H. Bowman, A. Leung, D. Needham, and D. Tirrel. 1996. Biomembrane templates for nanoscale conduits and networks. *Science*. 273:933–935.

Hirschberg, K., C. M. Miller, J. Ellenberg, J. F. Presley, E. D. Siggia, R. D. Phair, and J. L. Schwartz. 1998. Kinetic analysis of secretory protein traffic and characterization of golgi to plasma membrane transport intermediates in living cells. *J. Cell Biol.* 143:1485–1503.

Hochmuth, R. M., J.-Y. Shao, J. Dai, and M. P. Sheetz. 1996. Deformation and flow of membrane into tethers extracted from neuronal growth cones. *Biophys. J.* 70:358–369.

Karlsson, A., R. Karlsson, M. Karlsson, A.-S. Cans, A. Strömberg, F. Ryttsén, and O. Orwar. 2001. Molecular engineering: networks of nanotubes and containers. *Nature*. 409:150–152.

Karlsson, M., K. Sott, M. Davidson, A.-S. Cans, P. Linderholm, D. Chiu, and O. Orwar. 2002. Formation of geometrically complex lipid nanotube vesicle networks of higher-order topologies. *Proc. Natl. Acad. Sci. USA*. 99:11573–11578.

Landau, L. D., and E. M. Lifshitz. 1959. Fluid Mechanics. Pergamon Press, New York.

Powers, T. R., G. Huber, and R. E. Goldstein. 2002. Fluid-membrane tethers: Minimal surfaces and elastic boundary layers. *Phys. Rev. E*. 65:041901–041911.

Roopa, T., and G. V. Shivashankar. 2003. Nanomechanics of membrane tubulation and DNA assembly. *Appl. Phys. Lett*. 82:1631–1633.

Roux, A., G. Cappello, J. Cartaud, J. Prost, B. Goud, and P. Bassereau. 2002. A minimal system allowing tubulation with molecular motors pulling on giant liposomes. *Proc. Natl. Acad Sci. USA*. 99:5394–5399.

Saffinya, C. R. 2001. Structures of lipid-DNA complexes: supramolecular assembly and gene delivery. *Curr. Opin. Struct. Biol.* 11:440–448.

Sheetz, M. P. 2001. Cell control by membrane–cytoskeleton adhesion. *Nat. Rev. Mol. Cell. Biol.* 2:392–396.

Waters, M. G., and S. R. Pfeffer. 1999. Membrane tethering in intracellular transport. *Curr. Opin. Cell. Biol.* 11:453–459.

Waugh, R. E., and R. M. Hochmuth. 1987. Mechanical equilibrium of thick, hollow, liquid membrane cylinders. *Biophys. J.* 52:391–400.